

THREE-DIMENSIONAL NON-VACUUM PULSAR OUTER-GAP MODEL: LOCALIZED ACCELERATION
ELECTRIC FIELD IN THE HIGHER ALTITUDESKOUICHI HIROTANI¹

Academia Sinica, Institute of Astronomy and Astrophysics (ASIAA), PO Box 23-141, Taipei, Taiwan

ABSTRACT

We investigate the particle accelerator that arises in a rotating neutron-star magnetosphere. Solving the Poisson equation for the electro-static potential, the Boltzmann equations for relativistic electrons and positrons, and the radiative transfer equation simultaneously, we demonstrate that the electric field is substantially screened along the magnetic field lines by the pairs that are created and separated within the accelerator. As a result, the magnetic-field-aligned electric field is localized in the higher altitudes near the light cylinder and efficiently accelerates the positrons created in the lower altitudes outwards but not the electrons inwards. The resulting photon flux becomes predominantly outwards, leading to typical double-peak light curves, which are commonly observed from many high-energy pulsars.

Subject headings: gamma rays: stars — magnetic fields — methods: numerical — stars: neutron

1. INTRODUCTION

The Large Area Telescope (LAT) aboard the *Fermi Gamma-Ray Space Telescope* has detected 117 rotation-powered pulsars (Abdo et al. 2013)¹. The unprecedented amount of data for these γ -ray sources, allows us to study the statistical properties of the high-energy pulsars through the light-curve analysis. Adopting the polar-cap (PC) model (Sturrock 1971; Harding et al. 1978; Daugherty & Harding 1982; Dermer & Sturmer 1994), the slot-gap (SG) model (Arons 1983; Muslimov & Harding 2004; Dyks & Rudak 2003; Harding et al. 2005), and the outer gap (OG) model (Cheng et al. 1986a; Romani 1996; Cheng et al. 2000; Romani & Watters 2010), and comparing the predicted light-curve morphology with the observations (Dyks et al. 2004), they revealed that the SG model is geometrically favoured in some cases but the OG model is in other cases as opposed to the lower-altitude emission models such as the PC model (Romani & Watters 2010; Takata et al. 2011; Pierbattista et al. 2012, 2014; Johnson et al. 2014). Moreover, MAGIC and VERITAS experiments reported pulsed signals from the Crab pulsar up to 400 GeV (Aleksić et al. 2011a,b; Aliu et al. 2011, 2014), which indicates that such very-high-energy photons are probably emitted from the higher altitudes to avoid the strong magnetic absorption that would arise near the polar-cap (PC) surface.

In an OG, created pairs are separated by the magnetic-field-aligned electric field, E_{\parallel} . For middle-aged pulsars, pairs are mostly created near the inner boundary; thus, the out-going particles run much longer distance in the OG than the in-coming ones, resulting in an order of magnitude greater outward flux than the inward one (fig. 7 & 8 of Hirotani & Shibata (2002)). On the other hand, for relatively young pulsars such as the Vela pulsar, the outward γ -ray flux dominates the inward one by only several times (Takata et al. 2008), because the out-going particles run the strong- E_{\parallel} region several times

longer distance than the in-coming ones. However, such a non-negligible inward flux leads to the light curve that generally exhibits more than two peaks in a single neutron star rotation, which contradicts with observations.

Although it is unclear if the OG model does predict a dominant outward γ -ray flux for young or relatively young pulsars, they have assumed so to obtain the observed, double-peaked light curves (Romani & Yadigaroglu 1995; Cheng et al. 2000; Zhang & Cheng 2002; Takata & Chang 2007; Tang et al. 2008; Romani & Watters 2010; Bai & Spitkovski 2010a,b; Venter et al. 2012; Pierbattista et al. 2012, 2014; Johnson et al. 2014). We are, therefore, motivated by the need to contrive a more consistent OG model that quantifies the outward and inward γ -ray fluxes, incorporating the screening effect of E_{\parallel} by the created and separated charges in the gap. Extending the idea of Beskin (1992), Hirotani & Shibata (1999a,b) first solved the set of the non-vacuum Poisson equation, Boltzmann equations for electrons and positrons (e^{\pm}), and the radiative transfer equation simultaneously in a pulsar magnetosphere. It has been demonstrated (Takata et al. 2004; Hirotani 2006b, 2013) that a strong E_{\parallel} does arise between the null-charge surface and the light cylinder (LC), whose distance from the rotation axis is given by the light cylinder radius, $\varpi_{LC} = c/\Omega$, where c designates the speed of light and Ω the rotational frequency of the neutron star.

In the present letter, we numerically solve the non-vacuum OG electrodynamics in the three-dimensional (3-D) magnetosphere of a typical young pulsar and demonstrate that the outward photon flux naturally dominates the inward ones by virtue of the E_{\parallel} screening due to the separated motion of the created e^{\pm} s. Without loss of any generality, we can assume a positive E_{\parallel} ; in this case, e^{+} s are accelerated outwards while e^{-} s inwards, forming an outward current in the OG as a part of the global current circuit. We do not solve the global current closure issue, assuming a starward return current in the magnetic polar regions. We define the magnetic coordinates in § 2 and describe the 3-D vacuum OG model in § 3. We then

¹ For the latest Fermi discoveries, see also <https://confluence.slac.stanford.edu/display/GLAMCOG/Public+List+of+LAT-Detected+Gamma-Ray+Pulsars>

propose the new, 3-D non-vacuum OG model in § 4, and discuss some implications of this modern OG model in § 5.

2. 3-D MAGNETIC COORDINATES

In a rotating magnetosphere, the Poisson equation for the non-corotational potential Ψ becomes

$$-\nabla^2\Psi = 4\pi(\rho - \rho_{\text{GJ}}), \quad (1)$$

where ρ denotes the real charge density and the Goldreich-Julian (GJ) charge density is defined by

$$\rho_{\text{GJ}} \equiv -\frac{\mathbf{\Omega} \cdot \mathbf{B}}{2\pi c} + \frac{(\mathbf{\Omega} \times \mathbf{r}) \cdot (\nabla \times \mathbf{B})}{4\pi c}. \quad (2)$$

The acceleration electric field can be computed by

$$E_{\parallel} \equiv \mathbf{B} \cdot \mathbf{E} / B = -\partial\Psi/\partial s, \quad (3)$$

where s denotes the distance along the magnetic field line.

To specify the position in a three-dimensional (3-D) pulsar magnetosphere, it is convenient to introduce the magnetic coordinates (s, θ_*, φ_*) , where θ_* and φ_* represent the foot point of the field lines on the neutron star (NS) surface. Their relationship with the polar coordinates is given by equations (15)–(17) of Hirotani (2006a). The magnetic azimuthal angle φ_* is defined counter-clockwise around the magnetic dipole axis; $\varphi_* = 0$ points the opposite direction to the rotation axis from the magnetic axis on the two-dimensional poloidal plane in which both the rotation and magnetic axes reside. Thus, a negative φ_* represents a magnetic field line in the trailing side of a rotating magnetosphere, while a positive φ_* does that in the leading side.

As for the magnetic colatitudes θ_* , it is convenient to replace it with the dimensionless trans-field coordinate h such that

$$h \equiv 1 - \theta_*/\theta_*^{\text{max}}, \quad (4)$$

where $\theta_*^{\text{max}} = \theta_*^{\text{max}}(\varphi_*)$ describes the PC rim, outside of which the magnetic field lines close within the LC. In what follows, we use the coordinates (s, h, φ_*) to specify points in the 3-D magnetosphere. In an OG, E_{\parallel} vanishes on the last-open field line, $h = 0$. In the convex side of the magnetic field lines, E_{\parallel} increases nearly quadratically with increasing h at each (s, φ_*) , attain the maximum value near the central height $h = 0.5h_m$, then reduces to vanish above a certain height $h_m = h_m(s, \varphi_*)$, which forms the upper boundary of the OG. Here, the gap trans-field thickness h_m corresponds to f in Cheng et al. (1986a) and w in Romani (1996). Because E_{\parallel} is screened by the created pairs, we obtain $h_m \sim 0.1$ for very young pulsars like the Crab pulsar, while $h_m > 0.5$ for middle-aged pulsars like the Geminga pulsar. In the non-vacuum OG model, the upper boundary $h_m(s, \varphi_*)$ is consistently determined from the separating motion of the charges by the Poisson and the Boltzmann equations.

To describe the magnetic field, we adopt the vacuum rotating dipole solution (Cheng et al. 2000) in the entire simulation region. Although this approximation breaks down near and outside the LC (Spitkovski 2006), it properly gives the outward/inward flux ratio at least qualitatively, because the screening of E_{\parallel} takes place within the LC.

To solve the Poisson equation and the e^{\pm} Boltzmann equations, we adopt 300 bins in s direction (from the PC surface $s = 0$ to $s = 3\varpi_{\text{LC}}$ along each magnetic field line), 72 bins in h direction (from the lower boundary $h = 0$ to $h = 3h_{\text{max}}$), and 96 bins in φ_* direction (from $\varphi = -\pi$ to $\varphi = \pi$); here, h_{max} refers to the maximum value of $h_m(s, \varphi_*)$. The outer boundary of the gap is determined as the free boundary at which E_{\parallel} vanishes. For example, if the OG is vacuum ($\rho = 0$) and thin ($h_{\text{max}} \ll 1$), the outer boundary is located at the inflection point where the poloidal magnetic field configuration changes from convex to concave (eq. [68] of (Hirotani 2006a)). If the OG is non-vacuum or thick, we must solve the Poisson equation to find the outer boundary. Although there is no physical reason why an OG outer boundary should be located within the LC (because the LC is not a special place for any physical process), we impose that the maximum distance of the outer boundary from the rotation axis is $0.9\varpi_{\text{LC}}$ to take a consistency with classic OG models. To solve the radiative transfer equation, we employ the same magnetic coordinates as the Poisson and e^{\pm} Boltzmann equations with coarse grids: 25 bins in s direction (from $s = 0$ to $s = 3\varpi_{\text{LC}}$), 10 bins in h direction (from the lower boundary $h = 0$ to $h = 2.5h_{\text{max}}$, and 96 bins in φ_* direction (from $\varphi_* = -\pi$ to $\varphi_* = \pi$). In the momentum space, we adopt 43 bins for the photon energy (from 0.005 eV to 20 TeV), 40 bins for the latitudinal propagation direction (from 0 to π radian) with respect to the rotation axis, and 60 bins for the azimuthal propagation direction (from $-\pi$ to π radian).

We employ the minimal cooling scenario (Page et al. 2004), which has no enhanced cooling that could result from any of the direct Urca processes and adopts the standard equation of state, APR EOS (Akmal et al. 1998). In addition, in this letter, we assume that the NS envelope is composed of heavy elements (e.g., Fe, Co, Ni) with little accretion of light elements (e.g., H, He, C, O) from the atmosphere; in this case, the gap activity becomes most active (Hirotani 2013). We adopt the canonical NS mass of $1.4M_{\odot}$, and the magnetic dipole moment of $3.2 \times 10^{30} \text{ G cm}^3$. In this case, the NS radius becomes 11.6 km and the PC magnetic field strength does $4.1 \times 10^{12} \text{ G}$. To examine young pulsar emissions, we adopt $P = 54 \text{ ms}$ and $\dot{P} = 2.6 \times 10^{-13} \text{ s s}^{-1}$, which correspond to the NS age of 3 kyr if the spin down is due to the magnetic dipole radiation. To compute the flux, we adopt the distance of 1 kpc.

3. 3-D VACUUM OUTER GAP MODEL

Let us first examine a vacuum OG in the 3-D pulsar magnetosphere, by solving the Poisson equation (1) under $\rho = 0$, and by assuming $h_m = 0.08$, which is typical for young pulsars around 3 kyr (within the vacuum OG model). Since the Poisson equation is a second-order partial differential equation, and since the gap is transversely thin (i.e., $h_m \ll 1$), E_{\parallel} distributes quadratically in the trans-field direction, and maximizes at the middle height, $h = 0.5h_m = 0.04$. We plot this maximum value on the last-open-field-line surface, (s, φ_*) in figure 1. In this vacuum OG model, the inner (i.e., starward) boundary is located at the null-charge surface, whose intersection with the last-open-field-line surface is indicated by the white solid curve in figure 1.

It follows that E_{\parallel} peaks in the higher altitudes ($0.7 < s/\varpi_{\text{LC}} < 1.0$), particularly in the leading side ($45^{\circ} < \varphi_* < 75^{\circ}$). This is because the GJ charge density per magnetic flux tube has a greater gradient there compared to the lower altitudes or in the trailing side, as indicated by figure 1 of Hirotani (2014). This result forms a striking contrast to the standard OG models, which extends the 2-D solution of E_{\parallel} on the poloidal plane (i.e., at $\varphi_* = 0$) into the toroidal direction (i.e., to $\varphi_* \neq 0$ regions). It means that we must solve the Poisson equation fully three dimensionally even in the vacuum case.

Using this E_{\parallel} , we can solve the Boltzmann equations for e^{\pm} 's, and the emissivity distribution in the 3-D magnetosphere. Note that in a vacuum OG model, the Poisson equation is solved separately from the Boltzmann equations or the radiative transfer equations. The particles are accelerated up to the Lorentz factors $\gamma \sim 3 \times 10^7$ and efficiently emit GeV photons via the curvature process mainly within the OG, and less efficiently up-scatter the magnetospheric IR-UV photons into TeV after escaping from the OG, where the IR-UV photons are mostly emitted by the secondary pairs created outside the OG via the synchrotron process.

The resultant light curves are plotted in figure 2 for the three discrete viewing angles with respect to the rotation axis, $\zeta = 100^{\circ}$, 110° , and 120° . The solid lines represent the pulse profile of the outward-propagating γ -rays (emitted by positrons), while the dashed ones do that of the inward γ -rays (emitted by electrons). Note that the vacuum OG model predicts the detection of the inward emission from the southern OG in addition to the conventional outward emission from the northern OG. This forms a contrast to the two-pole caustic/SG model, which predicts the detection of only the outward emissions from the both poles, because the leptonic flux is outwardly uni-directional, and because sufficient emissivity is assumed below the null-charge surface. Since E_{\parallel} is stronger in the leading side, the leading peak (P1) tends to be stronger than the trailing peak (P2) at many observers' viewing angles, ζ .

Before escaping from the gap, typical inward-migrating electrons run $0.3\varpi_{\text{LC}}$, while typical outward-migrating positrons run $0.7\varpi_{\text{LC}}$. As a result, outward flux becomes only a few times stronger than the inward flux. Therefore, the light curve in figure 2 generally exhibits more than two peaks in a single NS rotation, which contradicts with the majority of gamma-ray observations.

4. 3-D NON-VACUUM OUTER GAP MODEL

Let us next consider the screening effect due to the separating motion of the created pairs in the gap. We solve equations (43)–(55) in Hirotani (2013) under the boundary conditions that e^{-} 's or e^{+} 's do not enter across either the inner or the outer boundaries. Pairs are mainly created when the inward curvature γ -rays collide with the outward thermal X-rays emitted from the NS surface. The created pairs in the gap are separated to screen E_{\parallel} to a small amplitude so that the pairs can be marginally separated. In this case, the real charge density has the same spatial gradient as the GJ charge density (Goldreich, & Julian 1969) along the magnetic field, as indicated by figure 5 of Hirotani (2006a). We neglect the magnetic-field deformation due to the mag-

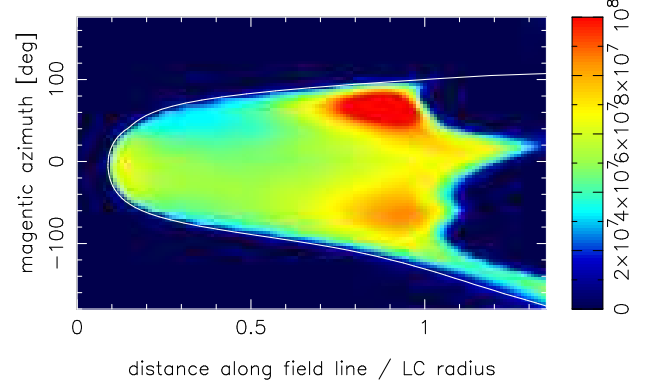


FIG. 1.— Acceleration electric field in the 3-D Vacuum OG model. The maximum value of E_{\parallel} [V m^{-1}] in the trans-field direction, is projected on the last-open-field-line surface at each (s, φ_*) .

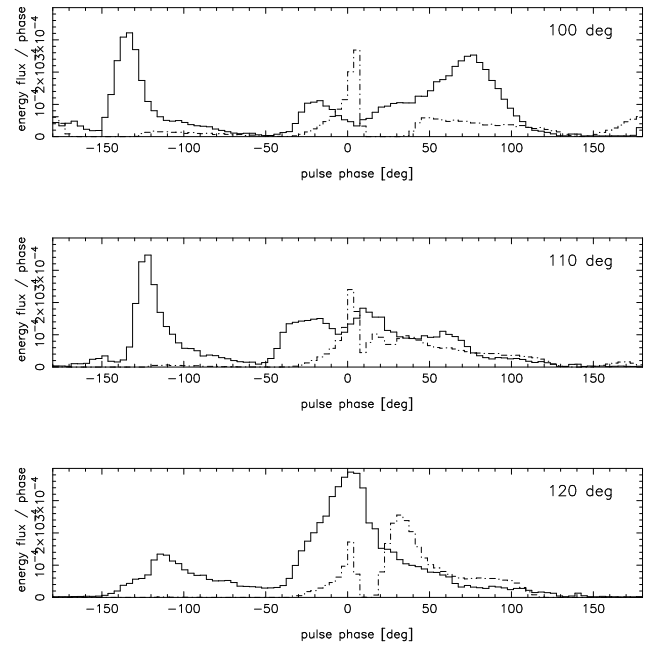


FIG. 2.— Gamma-ray pulse profiles above 91 MeV at three discrete viewing angles for the 3-D vacuum OG model. The thick curves represent the outward gamma-ray fluxes, while the thin ones do the inward fluxes. Photons are emitted not only within the light cylinder, but also outside of it by the positrons escaped from the gap. The ordinate ranges from 0 to $4 \times 10^{-4} \text{ MeV s}^{-1} \text{ cm}^{-2} \text{ deg}^{-1}$.

netospheric currents, adopting the same magnetic field geometry as in section 3.

Because of this screening effect, E_{\parallel} becomes very weak in the middle and lower altitudes, $s < 0.77\varpi_{\text{LC}}$, as figure 3 shows. It is also found that the regions that emit photons in P1 and P2 phases (i.e., in $50^{\circ} < \varphi_* < 80^{\circ}$ and $-105^{\circ} < \varphi_* < 45^{\circ}$ in fig. 3) have greater E_{\parallel} than other regions. The gap trans-field thickness becomes $0.11 < h_m < 0.13$ in most portions of the gap.

As a result of this E_{\parallel} screening, the outward photon flux dominates the inward one, as demonstrated by the light curves in figure 4. This is because the pairs are mostly created in the middle or the lower altitudes, $s < 0.77\varpi_{\text{LC}}$, which indicates that the positrons experience an efficient acceleration in the strong E_{\parallel} region in the higher altitudes while the electrons do not. There-

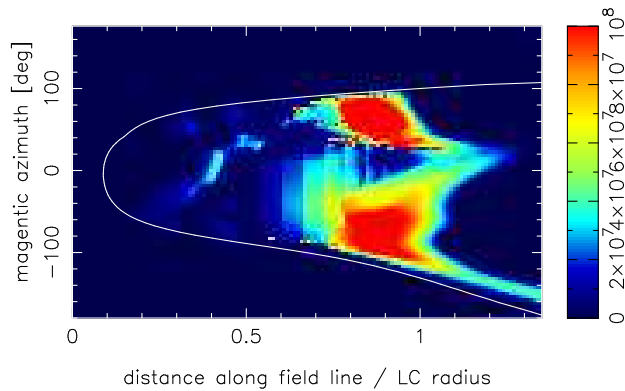


FIG. 3.— Same figure as figure 1, but the 3-D non-vacuum OG solution is plotted. The color code is common with figure 1.

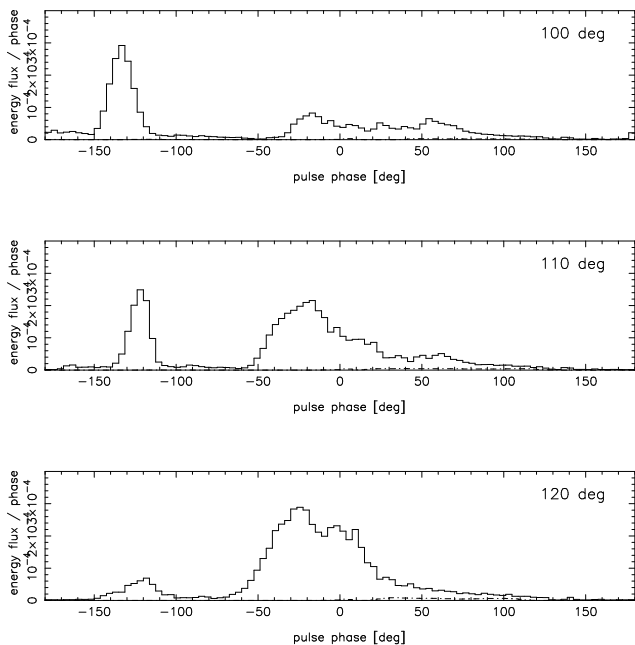


FIG. 4.— Same figure as figure 2, but the light curves for the 3-D non-vacuum OG solution is plotted. The ordinate range is same with figure 2. Note that only the outward flux (solid curve) appears in a non-vacuum OG model.

fore, the light curve is dominated by the outward photons, which are emitted from the northern OG into the southern hemisphere, and tends to exhibit a double-peak pulse profile for a wide range of ζ .

The expected phase-averaged spectrum is plotted for $\zeta = 110^\circ$ in figure 5. For comparison, we plot the spectrum of the outward and inward photons as the thick and thin curves, respectively. It is also confirmed from the figure that the gamma-ray flux is predominantly outward. As a result of the superposition of the curvature emission from different places with varying E_{\parallel} , between 0.16 GeV and 1.6 GeV, the νF_{ν} spectrum becomes a power-law with index 0.68, which is consistent with the Fermi observations of young pulsars. Since E_{\parallel} depends not only on (s, φ_*) , but also quadratically on h , it is essential to consider the superposition of the emission spectra along different magnetic field lines. The intrinsic luminosity of the magnetospheric emission is 1.7×10^{36} ergs s $^{-1}$ above 160 MeV, while it is 1.3×10^{35} ergs s $^{-1}$ below 160 MeV. The heated PC lu-

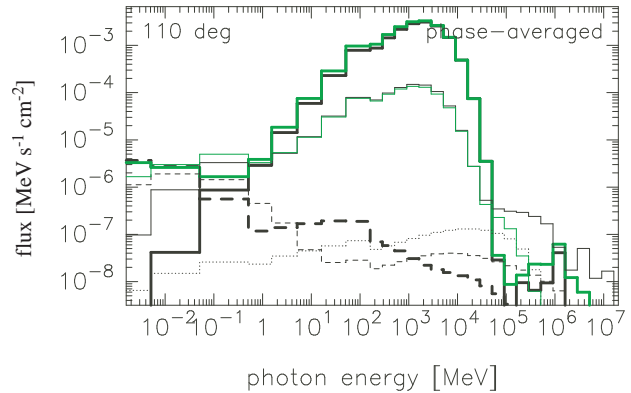


FIG. 5.— Non-vacuum, 3-D outer-gap solution: Phase-averaged spectrum at $\zeta = 110^\circ$. The thick lines represent the energy flux of outwardly emitted photons, while the thin ones do that of inward photons. The black solid, dashed, and dotted curves denote the spectrum of the primary, secondary, and tertiary photons, while the green solid ones do the final spectrum after absorption.

minosity is 3.3×10^{32} ergs s $^{-1}$. For comparison, the spin-down luminosity is 4.4×10^{37} ergs s $^{-1}$, and the cooling NS X-ray luminosity is 1.2×10^{33} ergs s $^{-1}$. The heated PC flux becomes greater than the magnetospheric X-ray flux if $\zeta < 45^\circ$ or $\zeta > 135^\circ$.

5. DISCUSSION

In summary, we have numerically examined the pulsar outer gaps, by solving the set of the Poisson equation, the e^{\pm} Boltzmann equations, and the radiative transfer equation from 0.005 eV to 20 TeV. Applying the method to a young pulsar with 3 kyr age, we find that the acceleration electric field E_{\parallel} is substantially screened by the separating motion of the created pairs, and that the γ -ray flux becomes predominantly outward due to the localization of E_{\parallel} in the higher altitudes. To reproduce the observed double-peak light curves, it is essential to solve the outer gap three-dimensionally, taking account of this screening effect.

As figure 4 indicates, the trailing peak has a long tail until the rotational phase of ~ 100 degrees. This is due to the emission from the trailing-most side of the magnetosphere ($\varphi_* < -90^\circ$) from a very high altitudes ($\varpi_{\text{LC}} < s < 3\varpi_{\text{LC}}$). Since the actual strength and direction of such emissions depend on the magnetic-field configuration near the LC, it could be possible to constrain the magnetic field configuration there. Figure 4 also shows that there is a strong emission component around $\varphi_* \sim -20^\circ$ (i.e., before P2). This component is suppressed, if we consider a very thin OG (e.g., $h_m < 0.05$), as suggested in the standard OG or SG models. However, if we solve the set of Maxwell-Boltzmann equations, we obtain $h_m \sim 0.12$ and the broad light curves as presented. It means that we cannot still reproduce the observed flux and sharp pulses simultaneously by the current particle accelerator models.

Let us briefly discuss an implication when the minimal cooling scenario with a heavy element envelope breaks down. If the NS envelope contains light elements with mass greatly exceeding $10^{-16} M_{\odot}$, the higher NS surface temperature (Page et al. 2004) leads to a reduction of h_m and hence the OG luminosity. On the contrary, if the cooling is dominated by neutrino emission via the direct Urca process, the resultant rapid cooling (in the initial

~ 100 years) (Negreiros et al. 2014; Coelho et al. 2014) will lead to an increase of h_m and hence the luminosity. In either case, we expect that $E_{||}$ is localized in the higher altitudes in the same way as demonstrated in this letter, by virtue of the strong negative-feedback effects in the OG electrodynamics (Hirotani 2006b)

Since the optical depth for photon-photon pair creation is around unity, the TeV photons created via the synchrotron-self-Compton process cannot be easily absorbed by the magnetospheric IR-UV photons, as indicated by the dashed and thick solid curves in figure 5. It suggests that we may expect relatively strong pulsed emissions around TeV from the pulsars of which inverse-Compton and photon-photon-absorption optical depths

are around unity, which is typical for young pulsars with ages around several thousand years. We will discuss this possibility in a separate paper.

The author is indebted to Drs. K. S. Cheng, J. Takata, and D. F. Torres for valuable discussion. This work is supported by the Theoretical Institute for Advanced Research in Astrophysics (TIARA) operated under Academia Sinica, and the Formosa Program between National Science Council in Taiwan and Consejo Superior de Investigaciones Científicas in Spain administered through grant number NSC100-2923-M-007-001-MY3.

REFERENCES

- Abdo, A. A. et al., 2013, *ApJS*, 208, 17
Aleksić, J. *et al.* 2011a, *ApJ*, 742, 43
Aleksić, J., *et al.* 2011b, *A&A*, 540, 69
Aliu, E., Arlen, T., Aune, T., *et al.* 2011, *Science* 334, 69
Aliu, E., Arlen, T., Aune, T., *et al.* 2014, *A&A*, 565, L12
Arons, J. 1983, *ApJ*, 266, 215
Bai, X. N. & Spitkovski, A. 2010a, *ApJ*, 715, 1270
Bai, X. N. & Spitkovski, A. 2010b, *ApJ*, 715, 1282
Beskin, V., Ishtomin, Ya. N. & Par'ev, V. I. 1992, *Soviet Astron.* 36, 642
Cheng, K. S., Ho, C. & Ruderman, M. 1986, *ApJ*, 300, 500
Cheng, K. S., Ruderman, M. & Zhang, L. 2000, *ApJ*, 537, 964
Coelho, E. L., Chiapparini, M., Bracco, M. E. & Negreiros, R. P. 2014, *Astron. Nachr.*, 335, 630
Daugherty, J. K. & Harding, A. K. 1982, *ApJ*, 252, 337
Dermer, C. D. & Sturmer, S. J. 1994, *ApJ*, 420, L75
Dyks, J., & Rudak, B. 2003, *ApJ*, 598, 1201
Dyks, J., Harding, A. K. & Rudak, B. 2004, *ApJ*, 606, 1125
Goldreich, P. & Julian, W. H. 1969, *ApJ*, 157, 869
Harding, A. K., Tademaru, E. & Esposito, L. S. 1978, *ApJ*, 225, 226
Harding, A. K. et al. 2005, *ApJ*, 622, 531
Hirotani, K. 2000, *MNRAS*, 317, 225
Hirotani, K. 2006a, *ApJ*, 652, 1475
Hirotani, K. 2006b, *Mod. Phys. Lett. A (Brief Review)* 21, 1319
Hirotani, K. 2013, *ApJ*, 766, 98
Hirotani, K. 2014, *MNRAS*, 442, L43
Hirotani, K. & Shibata, S., 1999a, *MNRAS*, 308, 54
Hirotani, K. & Shibata, S., 1999b, *MNRAS*, 308, 67
Hirotani, K. & Shibata, S., 2002, *ApJ*, 564, 369
Johnson, T. J., Venter, C., Harding, A. K., Guillemot, L., Smith, D. A., Kramer, M., elik, Ö., den Hartog, P. R. 2014, *ApJS*, 213, 6
Muslimov, A. & Harding, A. K. 2004, *ApJ*, 606, 1143
Negreiros, R.; Schramm, S.; Weber, F. 2014, *Astron. Nachr.*, 335, 703
Page, D., Lattimer, J. M., Prakash, M. & Steiner A. W. 2004, *ApJS*, 155, 623
Pierbattista, M., Grenier, I. A., Harding, A. K., Gonthier, P. L. 2012, *A&A*, 545, 42
Pierbattista, M., Harding, A. K., Grenier, I. A., Johnson, T. J., Caraveo, P. A., Kerr, M., & Gonthier, P. L. 2014, *A&A*, in press
Romani, R. W., & Yadigaroglu, I. A. 1995, *ApJ*, 438, 314
Romani, R. W. 1996, *ApJ*, 470, 469
Romani, R. & Watters, K. P. 2010, *ApJ*, 714, 810
Spitkovsky, A. 2006, *ApJ*, 648, L51
Sturrock, P. A. 1971, *ApJ*, 164, 529
Takata, J., Shibata, S., & Hirotani, K. 2004, *MNRAS*, 354, 1120
Takata, J., Wang, H.-K. & Shibata, S. 2008, *MNRAS*, 386, 748
Takata, J., Chang, H.-K. 2007, *ApJ*, 670, 677
Takata, J., Wang, Y. & Cheng, K. S. 2011, *ApJ*, 726, 44
Tang, A. P. S., Takata, J., Jia, J. J. & Cheng, K. S. 2008, *ApJ*, 676, 562
Venter, C., Johnson, T. J. & Harding, A. K. 2012, *ApJ*, 744, 34
Zhang, J. L. & Cheng, K. S. 2002, *ApJ*, 2002, 872